

Enhanced voltage-controlled magnetic anisotropy via magneto-elasticity in FePt/MgO(001)

Qurat-ul-ain¹, D. Odkhuu², S. H. Rhim^{1,*} and S. C. Hong^{1†}

¹Department of Physics and Energy Harvest-Storage Research Center, University of Ulsan, Ulsan, Republic of Korea

²Department of Physics, Incheon National University, Incheon, Republic of Korea

(Dated: January 7, 2020)

The interplay between magneto-electricity (ME) and magneto-elasticity (MEL) is studied in the context of voltage-controlled magnetic anisotropy (VCMA). Strain plays more than a role of changing lattice constant but that of the internal electric field in the heterostructure. As a prototype, FePt/MgO(001) is visited, where the behavior of two interfaces are drastically different: one exhibits switching the other does not. Whether an external electric field (E_{ext}) is present or not, we found VCMA coefficient larger than 1 pJ/V·m, as a consequence of the rearrangement of d orbitals with $m = \pm 1$ and ± 2 in response to an external electric field. In addition, magneto-crystalline anisotropy (MA) is analyzed with strain taken into account, where non-linear feature is presented only accountable by invoking second-order MEL.

I. Introduction

The advent of spintronics has witnessed a realization of magnetic random access memory (MRAM), which compliments or replaces conventional memories. This progress has relied on giant magneto-resistance (GMR)^{1,2} and tunnel magneto-resistance (TMR)^{3,4}. Moreover, the advancement is further pushed forward with the incorporation of spin-transfer torque (STT)⁵⁻⁷ and spin-orbit torque (SOT)^{8,9} for magnetization switching. In all cases, perpendicular magneto-crystalline anisotropy (PMA) is an essential ingredient to guarantee high bit density, lower switching current (I_{SW}), and thermal stability, $\Delta = KV/k_B T$, where K is anisotropy; k_B is the Boltzmann constant; T is temperature. In spite of notable success in MRAM, high I_{SW} for switching and associated Joule heating are major obstacles to overcome.

Magneto-electric random access memory (MeRAM) has emerged as an alternative or compliments to MRAM, which utilizes voltage-controlled magnetic anisotropy (VCMA), where an external electric field (E_{ext}) manipulates switching from one magnetization state to the other. The efficiency of VCMA is characterized by a single parameter, the VCMA coefficient, $\beta = \Delta E_{MA}/\Delta E_{eff}$. The effective electric field, $E_{eff} = E_{ext}/\epsilon_{\perp}$, where ϵ_{\perp} is the out-of-plane component of the dielectric tensor of an insulator, and E_{MA} is the magneto-crystalline anisotropy energy. In the pursuit of VCMA, various heterostructures have been explored, where FePt/MgO is one choice. $L1_0$ FePt is ferromagnetic with a high Curie temperature of 750 K¹⁰ and MgO has widely been used substrate. In addition to E_{ext} , strain can be another driving force of VCMA, which influences β through ϵ_{\perp} of the insulator or acts as an effective electric field at ferromagnetic-insulator interface even in the absence of E_{ext} . Hence, comparative studies of VCMA with and without strain would be intriguing.

In this work, magneto-electricity (ME) as well as magneto-elasticity (MEL) of FePt/MgO is investigated. The non-linear magneto-crystalline anisotropy as a function of strain (η) is explained by invoking second-order MEL contribution, which is usually ignored. Fe-interface shows spin-reorientation for $4.5 < \eta < 7\%$ while for Pt case MA is positive regardless of η . This difference stems from the competition between the positive effective anisotropy and negative first-order magneto-elasticity. Later, extremely large β of FePt/MgO is presented

as a result of an interplay between η and E_{ext} . More specifically, the rearrangement of d orbitals at the interface in response to E_{ext} is the key, whose details are analyzed with band- and atom-resolved decompositions of MA.

II. Computational methods

First-principles calculations have been carried out using Vienna *ab initio* Simulation Package (VASP) package¹¹ with projector augmented wave (PAW) basis¹². Generalized gradient approximation is employed for the exchange-correlation potential¹³. Cutoff of 500 eV for plane wave expansion and a $12 \times 12 \times 1$ k mesh are used.

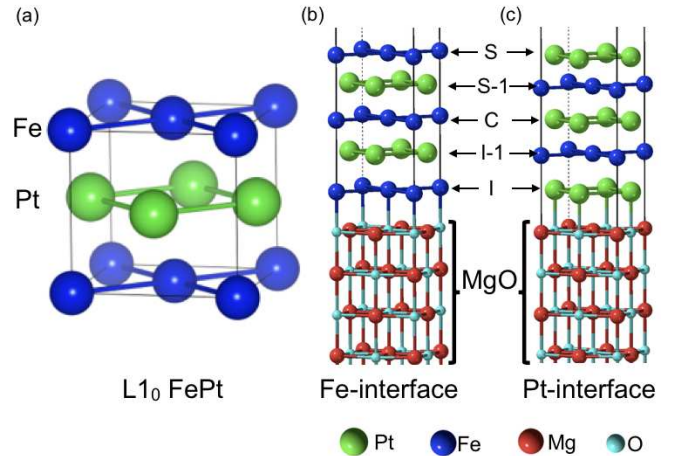


FIG. 1. (a) Bulk FePt $L1_0$ structure. 5 MLs of FePt on 8 MLs MgO (001) with (b) Fe- and (c) Pt-interface, respectively. Blue, green, cyan and red spheres represent Fe, Pt, O and Mg atoms, respectively. Surface, sub-surface, center, interface, and sub-interface layers are denoted by S , $S-1$, C , I , and $I-1$

Fig. 1 shows the structure of bulk FePt and FePt/MgO film. Bulk FePt has $L1_0$ structure [Fig. 1(a)] while the film consists of 5 monolayers (MLs) of FePt on 8 MLs MgO(001) [Fig. 1(b) and (c)]. In film, two different interfaces are taken into account by placing (i) Fe atoms on top of O atoms [Fig. 1(b)]

and (ii) Pt atoms on top of O atoms [Fig. 1(c)], which are referred to Fe- and Pt-interface, respectively. The vacuum region of 12 Å is taken between adjacent cells. Both interfaces are systematically studied, where *S*, *S*-1, *C*, *I*, and *I*-1 refer to the surface, sub-surface, center, interface, and sub-interface layer, respectively. The optimized lattice constant of FePt and MgO are 3.864 and 4.212 Å, respectively, resulting in a large tensile strain (η) \sim 8.2% on the FePt layer, assuming the MgO substrate is unstrained. In order to study strain dependent MA of the system, η , defined as $(a - a_{FePt})/a_{FePt}$, is varied from 0% (unstrained FePt lattice constant) to 8% (nearly unstrained MgO lattice constant), where a_{FePt} is the equilibrium lattice constant of bulk FePt. Interlayer distances are relaxed for each strain with force criteria 1×10^{-3} eV/Å. Magneto-crystalline anisotropy energy (E_{MA}) is determined from the total energy difference between [100] and [001] directions, where spin-orbit coupling (SOC) is treated in second-variational way¹⁴. Convergence of E_{MA} is checked with $30 \times 30 \times 1$ k mesh. The electric field along the surface normal is applied employing dipole layer method¹⁵. In this work, shape anisotropy is not included in magnetic anisotropy.

III. Results and Discussion

When $\eta = 0\%$, $E_{MA} = 12.4$ and 21.5 erg/cm² for Fe- and Pt-interface, respectively, indicating perpendicular magnetization. Under tensile strain, both interfaces exhibit parabolic curve as shown in Fig. 2(a) and (b). However, one interface shows switching behavior but the other does not. For Fe-interface $E_{MA} < 0$ for $4.5 < \eta < 7\%$, whereas for Pt-interface

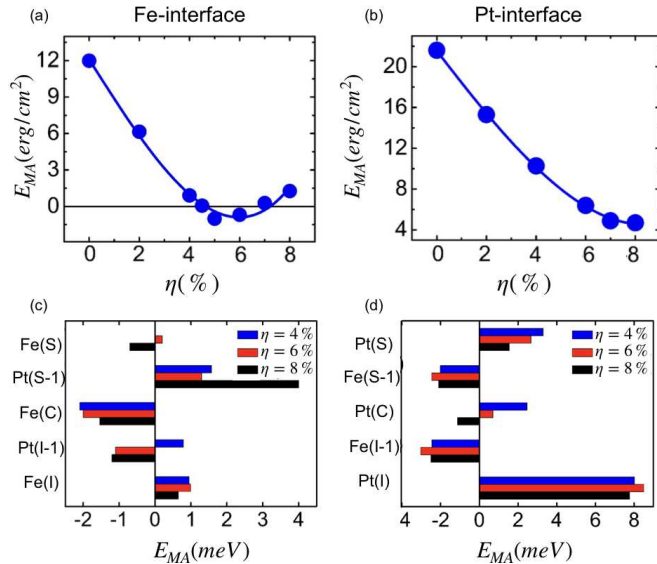


FIG. 2. E_{MA} as a function of η for (a) Fe- and (b) Pt-interface. Circles denote calculations and solid line represents fitting curve according to Eq. 2. Atomic layer decomposed E_{MA} for (c) Fe- and (d) Pt-interface, respectively. Blue, red, and black bars represent $\eta = 4, 6$ and 8% , respectively

E_{MA} decreases with strain. The overall feature is expressed as

$$E_{MA} = E_{MA}^0 + b_1 t \sum_{k=1}^3 \eta_k \alpha_k^2 + \frac{1}{2} B_1 t \sum_{k=1}^3 \eta_k^2 \alpha_k^2, \quad (1)$$

where E_{MA}^0 is the zero strain anisotropy energy per area; α_k and η_k ($k = 1, 2, 3$) are the direction cosines of magnetization and the strain tensor, respectively; t is the FM film thickness; b_1 and B_1 are the first- and second-order MEL coefficients, respectively¹⁶.

MEL energy is expanded up to second-order of η , whose coefficient B_1 is usually small and ignored^{17,18}. However, it is explicitly taken into account here, whose consequence is discussed later. The zero-strain anisotropy energy is approximated as $K_1 t (1 - \alpha_3^2)$ for uniaxial symmetry. It is decomposed into bulk and interface contributions, $K_1 = K_1^v + K_1^i/t \approx K_1^i/t$ for thin film limit. In tetragonal structure, $\eta_1 = \eta_2 = \eta$ and the perpendicular strain η_3 is determined from magneto-elastic equation of state [See Supplementary Information]. Substituting the calculated strain value in Eq. (1) gives

$$E_{MA} = K_{eff} + (1 + \omega) b_1 t \eta + (1 - \omega) \frac{B_1}{2} t \eta^2, \quad (2)$$

where

$$K_{eff} = K_1^i + \omega \frac{b_1^2}{c_{11}} \left(1 + \frac{B_1}{2c_{11}} \right) t, \quad (3)$$

and

$$\omega = c_{11}^2 / (c_{11} + B_1)^2. \quad (4)$$

where c_{11} is the elastic stiffness constant at constant magnetization. The derivation of Eq. (2) is also given in Supplementary Information.

Table I lists magneto-elastic and effective anisotropy coefficients, extracted by fitting *ab initio* results. The second-order term, B_1 , responsible for the non-linearity is significantly large with 1.29 and 0.79×10^8 erg/cm³ for Fe- and Pt-interface, respectively. The difference in magnitudes of B_1 for both interfaces arises due to different local environment of two interfaces. Fe atoms experience larger magneto-elasticity in the presence of MgO substrate than Pt interface. The difference of two interfaces is further discussed now.

TABLE I. First-order (b_1) and second-order (B_1) bulk magneto-elastic coefficients in ($\times 10^8$ erg/cm³), and effective anisotropy (K_{eff}) coefficient in (erg/cm²) for Fe- and Pt-interface, respectively.

Interface	b_1	B_1	K_{eff}
Fe	-3.16	1.29	12.44
Pt	-2.43	0.79	21.57

The calculated B_1 is of the opposite sign to that of b_1 for both interfaces. Further, it has been asserted that in the presence of strain, $b_1(\eta) = b_1 + B_1 \eta$ ^{19,20}. In our study, the ratio $|B_1/b_1|$ is large for Fe-interface as compared to Pt-interface, leading to a change in sign of b_1 for large strain values. For the Fe-interface, a competition between K_{eff} and $b_1 \cdot t$ produces

spin reorientation, for $4.5 < \eta < 7\%$. On the other hand, for the Pt-interface, $K_{eff} > b_1 \cdot t$ results in PMA for η up to 8%.

Due to spin reorientation transition, we focus on $\eta = 4, 6,$ and 8% . Fig. 2(c-d) provides atomic layer resolved E_{MA} . PMA mainly arises from Pt layers. Especially, the dominant PMA contribution comes from Pt(S-1) for Fe-interface and from Pt(I) for Pt-interface. Pt contribution to PMA is consistent with hard X-ray photoemission experiment²¹. On the contrary, Fe atoms mostly contribute to $E_{MA} < 0$, except Fe(I) and Fe(S) layers. Under strain, the overall behavior of E_{MA} remains the same for most of the atoms with changes in magnitude only. PMA from Fe(S), Pt(I-1) and Pt(C) at $\eta = 4\%$ becomes in-plane as η approaches to 8%.

Now switching to VCMA, Fig. 3 shows change in MA as a function of E_{eff} for $\eta = 4, 6,$ and 8% . VCMA coefficient is defined as $\beta = \frac{\Delta E_{MA}}{\Delta E_{eff}}$ in the linear regime of E_{eff} as mentioned earlier. We choose $\epsilon_{\perp}/\epsilon_o = 20.0, 12.0, 9.8$ for MgO when $\eta = 4, 6,$ and 8% , respectively, taken from Ref.²². Large VCMA coefficients are found for both interfaces. For Pt-interface, $\beta = -1.24, -1.35,$ and -1.36 pJ/(V·m) under $\eta = 4, 6,$ and 8% , respectively. On the other hand, Fe-interface exhibits qualitatively different VCMA with strain. The V-shape curve is apparent for $\eta = 4$ and 6% with $\beta = 1.70$ (-0.44) and 0.79 (-1.53) when $E_{eff} > 0$ ($E_{eff} < 0$), respectively. At $\eta = 8\%$, the VCMA curve changes to Λ -shape with $\beta = -1.77$ (1.68) under $E_{eff} > 0$ ($E_{eff} < 0$).

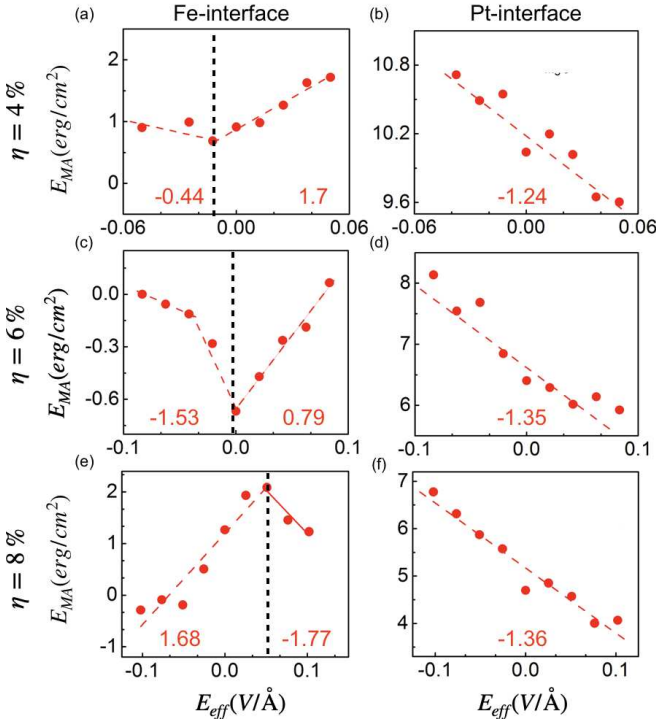


FIG. 3. VCMA of FePt/MgO heterostructure at different strain values for Fe- (left-panel) and Pt-interface (right-panel), respectively. Upper, middle, and lower row represent strain (η) of 4, 6, and 8%, respectively. VCMA coefficient are denoted inside each plot.

To understand the underlying mechanism of strain-induced

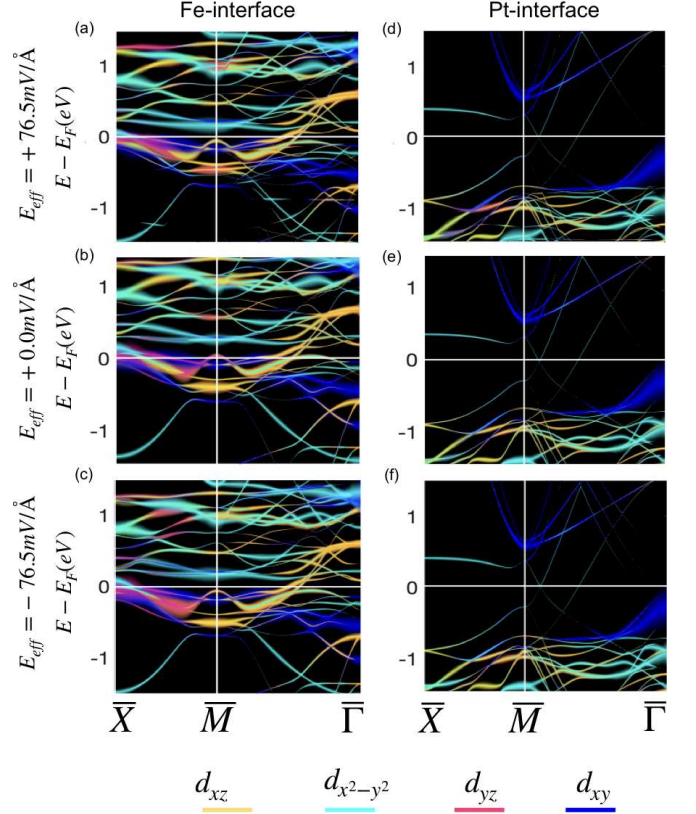


FIG. 4. Orbital resolved interfacial (a-c) Fe d bands for minority spin, (d-f) Pt d bands for majority spin along $\bar{X}-\bar{M}-\bar{\Gamma}$ at $\eta = 8\%$ under $E_{eff} = +76.5, 0, -76.5$ mV/Å. Blue, cyan, pink, and yellow for $d_{xy}, d_{x^2-y^2}, d_{yz},$ and d_{xz} . The d_{z^2} bands can contribute negatively to PMA and are not plotted here.

MA and VCMA, orbital resolved bands at $\eta = 8\%$ are plotted in Fig. 4 along high symmetry lines in two-dimensional Brillouin zone (BZ) under $E_{eff} = +76.5, 0,$ and -76.5 mV/Å. The $\eta = 8\%$ case are discussed in detail as it shows largest VCMA coefficient. For Fe- and Pt-interfaces, only the minority spin channel of Fe d bands and majority spin channel of Pt d bands are presented, respectively, as other spin channels do not contribute significantly to PMA. The d_{z^2} orbitals for both interfaces can contribute negatively to PMA and are shown in Supplementary Information. Both spin channels for Fe and Pt d bands at $\eta = 8\%, 6\%$, and 4% are also provided in Fig. S1 and Fig. S2 in Supplementary Information, respectively.

In the framework of perturbation theory²³, positive (negative) E_{MA} comes from spin-orbit coupling (SOC) between the unoccupied and occupied majority or minority spin states with the same (different) magnetic quantum number through ℓ_z (ℓ_x). This approach has been widely applied in various systems²⁴⁻²⁹.

First, we discuss without E_{ext} , namely, strain-induced MA. For Fe-interface, $E_{MA} > 0$ arises from $\langle d_{xy} \downarrow | \ell_z | d_{x^2-y^2} \downarrow \rangle$ and $\langle d_{yz} \downarrow | \ell_z | d_{xz} \downarrow \rangle$ along $\bar{X}\bar{M}$ [Fig. 4(b)]. Similarly, for Pt-interface $E_{MA} > 0$ mainly comes from $\langle d_{x^2-y^2} \uparrow | \ell_z | d_{xy} \uparrow \rangle$ along $\bar{M}\bar{\Gamma}$ [Fig. 4(e)]. As tensile strain decreases, d bands experi-

ence overall downward shift for Fe-interface. However, for Pt-interface, d_{xy} and $d_{x^2-y^2}$ moves upward and downward, respectively, with decreasing strain, which is shown in Fig. ?? and Fig. ?? in Supplementary Information. Strain driven band rearrangement leads to substantial change in E_{MA} as $E_{MA} \propto \Delta = 1/(e_u - e_o)$, where e_u (e_o) denotes energies of unoccupied (occupied) bands. In particular, at $\eta = 6\%$ for Fe-interface, $E_{MA} < 0$ comes from $\langle d_{yz} \downarrow | \ell_x | d_{xy} \downarrow \rangle$ around $\frac{1}{2}\overline{XM}$. Also, at $\eta = 8\%$, $E_{MA} > 0$ is through $\langle d_{xy} \downarrow | \ell_z | d_{x^2-y^2} \downarrow \rangle$ around \overline{X} .

Moving to VCMA, bands shift at $\eta = 8\%$ under $E_{eff} = \pm 76.5 \text{ mV/\AA}$ are shown in top and bottom panels of Fig. 4. To understand in a simple picture, a schematic diagram is illustrated in Fig. 5. $\Delta^\alpha = 1/(e_u - e_o)$ ($\alpha = +, 0, -$) denotes the inverse of the energy difference between unoccupied and occupied bands when E_{eff} is positive, zero, and negative, respectively.

Summing all SOC matrices, $\Delta^0 > \Delta^+ > \Delta^-$ justifies the Λ -shaped VCMA for Fe-interface. Under zero-field, occupied $d_{x^2-y^2}$ (d_{xz}) bands couples with unoccupied d_{xy} (d_{yz}) bands at $\frac{1}{2}\overline{XM}$, giving $E_{MA} > 0$. With $E_{eff} = \pm 76.5 \text{ mV/\AA}$, unoccupied bands d_{xy} and d_{yz} becomes occupied, resulting in $E_{MA} = 0$. Moreover, when $E_{eff} > 0$, d_{xy} and d_{xz} occupied bands along with $d_{x^2-y^2}$ and d_{yz} unoccupied bands move towards E_F at \overline{X} and \overline{M} , providing large PMA. While when $E_{eff} < 0$, these bands moves away from E_F , as a result contributing small PMA. On the other hand, for Pt-interface, $\Delta^- > \Delta^0 > \Delta^+$ explains linear VCMA. When $E_{eff} < 0$, the unoccupied d_{xy} band and occupied $d_{x^2-y^2}$ band at \overline{X} , shift towards E_F with respect to zero-field, resulting in enhanced PMA. However, when $E_{eff} > 0$, both these bands move away from E_F as compared to zero-field, hence PMA is reduced.

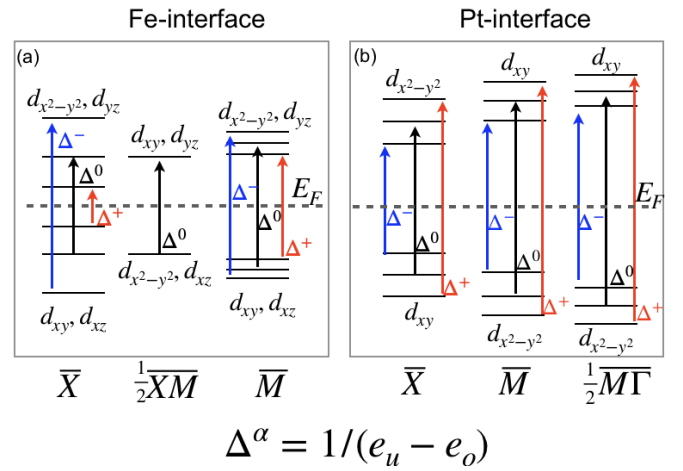


FIG. 5. Schematic diagram of bands shift under E_{eff} . $\Delta^\alpha = \frac{1}{e_u - e_o}$ represents the strength of SOC, where e_u (e_o) are energies of unoccupied (occupied) band; $\alpha = +, 0, -$ denotes when $E_{eff} > 0$, $E_{eff} = 0$, and $E_{eff} < 0$, respectively. Vertical arrows indicates possible coupling responsible for PMA.

IV. Conclusions

In summary, we investigated strain dependent voltage-controlled magnetic anisotropy for both Fe- and Pt-interfaces of FePt/MgO(001) film using *ab initio* electronic structure calculations. We predicted a huge VCMA coefficient $\sim 1.77 \text{ pJ/(V}\cdot\text{m)}$ due to the internal electric field as a result of strain. Moreover, magneto-crystalline anisotropy as a function of strain is also discussed. The strain-dependent non-linear magneto-crystalline anisotropy is explained by invoking second-order magneto-elastic (MEL) term in MA energy. Fe-interface shows spin-reorientation for $4.5 < \eta < 7\%$ as a consequence of the competition between the positive K_{eff} and negative $b_1 \cdot t$. Magneto-crystalline anisotropy turns out to be extremely sensitive to strain and interface. Our finding provides a direction for experiments to achieve enhanced VCMA coefficient along with large PMA for ultra-low power non-volatile memory devices.

Acknowledgments

This work was supported by National Research Foundation of Korea (NRF) grant (NRF-2018R1A4A1020696 and NRF-2019R1I1A3A01059880).

* Email address: sonny@ulsan.ac.kr

† Email address: schong@ulsan.ac.kr

¹ G. Binasch, P. Grünberg, F. Saurenbach, and W. Zinn, Phys. Rev. B **39**, 4828 (1989).

² M. N. Baibich, J. M. Broto, A. Fert, F. N. Van Dau, F. Petroff, P. Etienne, G. Creuzet, A. Friederich, and J. Chazelas, Phys. Rev. Lett. **61**, 2472 (1988).

³ M. Julliere, Phys. Lett. A **54**, 225 (1975).

⁴ S. S. Parkin, C. Kaiser, A. Panchula, P. M. Rice, B. Hughes, M. Samant, and S.-H. Yang, Nat. Mater. **3**, 862 (2004).

⁵ J. C. Slonczewski, J. Magn. Magn. Mater. **159**, L1 (1996).

⁶ L. Berger, Phys. Rev. B **54**, 9353 (1996).

⁷ M. Tsoi, A. Jansen, J. Bass, W.-C. Chiang, V. Tsoi, and P. Wyder, Nature **406**, 46 (2000).

⁸ Y.-W. Oh, S.-h. C. Baek, Y. M. Kim, H. Y. Lee, K.-D. Lee, C.-G. Yang, E.-S. Park, K.-S. Lee, K.-W. Kim, G. Go, *et al.*, Nat.

- Nanotechnol. **11**, 878 (2016).
- ⁹ X. Qiu, P. Deorani, K. Narayanapillai, K.-S. Lee, K.-J. Lee, H.-W. Lee, and H. Yang, *Sci. Rep.* **4**, 4491 (2014).
 - ¹⁰ D. Xu, C.-J. Sun, J.-S. Chen, T.-J. Zhou, S. M. Heald, A. Bergman, B. Sanyal, and G. M. Chow, *J. Appl. Phys.* **116**, 143902 (2014).
 - ¹¹ G. Kresse and J. Furthmüller, *Phys. Rev. B* **54**, 11169 (1996).
 - ¹² P. E. Blöchl, *Phys. Rev. B* **50**, 17953 (1994).
 - ¹³ J. Perdew and Y. Wang, *Phys. Rev. B* **45**, 13244 (1992).
 - ¹⁴ D. Koelling and B. Harmon, *J. Phys. C:Solid State Phys.* **10**, 3107 (1977).
 - ¹⁵ J. Neugebauer and M. Scheffler, *Phys. Rev. B* **46**, 16067 (1992).
 - ¹⁶ L. D. Landau and E. M. Lifshitz, *Electrodynamics of Continuous Media (Pergamon Press, Oxford, 1984)* (Pergamon Oxford, 1984).
 - ¹⁷ A. Shick, D. Novikov, and A. J. Freeman, *Phys. Rev. B* **56**, R14259 (1997).
 - ¹⁸ V. Z. Paes and D. H. Mosca, *J. Magn. Magn. Mater.* **330**, 81 (2013).
 - ¹⁹ M. Komelj and M. Fähnle, *J. Magn. Magn. Mater.* **222**, 245 (2000).
 - ²⁰ Z. Tian, D. Sander, and J. Kirschner, *Phys. Rev. B* **79**, 024432 (2009).
 - ²¹ S. Ueda, M. Mizuguchi, Y. Miura, J. Kang, M. Shirai, and K. Takanashi, *Appl. Phys. Lett.* **109**, 042404 (2016).
 - ²² P. Ong, N. Kioussis, D. Odkhuu, P. K. Amiri, K. Wang, and G. P. Carman, *Phys. Rev. B* **92**, 020407 (2015).
 - ²³ D. S. Wang, R. Wu, and A. J. Freeman, *Phys. Rev. B* **47**, 14932 (1993).
 - ²⁴ K. Nakamura, T. Akiyama, T. Ito, M. Weinert, and A. J. Freeman, *Phys. Rev. B* **81**, 220409(R) (2010).
 - ²⁵ D. Odkhuu, W. S. Yun, S. H. Rhim, and S. C. Hong, *Appl. Phys. Lett.* **98**, 152502 (2011).
 - ²⁶ D. Odkhuu, S. H. Rhim, N. Park, and S. C. Hong, *Phys. Rev. B* **88**, 184405 (2013).
 - ²⁷ K. Hotta, K. Nakamura, T. Akiyama, T. Ito, T. Oguchi, and A. J. Freeman, *Phys. Rev. Lett.* **110**, 267206 (2013).
 - ²⁸ D. Odkhuu, W. S. Yun, S. H. Rhim, and S. C. Hong, *J. Magn. Magn. Mater.* **414**, 126 (2016).
 - ²⁹ Qurat-ul-ain, D. D. Cuong, D. Odkhuu, S. H. Rhim, and S. C. Hong, *J. Magn. Magn. Mater.* **467**, 69 (2018).

Supplementary Material:

Qurat-ul-ain¹, D. Odkhuu², S. H. Rhim^{1,*} and S. C. Hong^{1†}

¹*Department of Physics and Energy Harvest-Storage Research Center,*

University of Ulsan, Ulsan, Republic of Korea

²*Department of Physics, Incheon National University, Incheon, Republic of Korea*

(Dated: January 7, 2020)

Derivation of magneto-crystalline anisotropy energy density

The magneto-crystalline anisotropy energy (E_{MA}) is written as

$$E_{MA} = K_1 t (1 - \alpha_3^2) + b_1 t \sum_{k=1}^3 \eta_k \alpha_k^2 + \frac{1}{2} B_1 t \sum_{k=1}^3 \eta_k^2 \alpha_k^2, \quad (1)$$

where the first-term is the zero strain anisotropy energy and the latter two are the magneto-elastic energy terms[1]. As mentioned in the main text, K_1 is the anisotropy constant, α_k ($k = 1, 2, 3$) are the direction cosines of magnetization with respect to the principal axis, b_1 and B_1 are the first- and second-order magneto-elastic coefficients, respectively[2], and η_k ($k = 1 - 6$) is the strain tensor in Voigt's notation. For a thin film grown epitaxially along the [001] crystallographic directions, shear strains, i.e., $\eta_4 = \eta_5 = \eta_6 = 0$ and $\eta_1 = \eta_2 = \eta$ due to tetragonal symmetry. The lattice strain η_k in Eq. 1 can be calculated via boundary conditions of the problem using the magneto-elastic equation of state, given as:

$$\sigma_k = \frac{\partial}{\partial \eta_k} \left(b_1 t \sum_{k=1}^3 \eta_k \alpha_k^2 + \frac{1}{2} B_1 t \sum_{k=1}^3 \eta_k^2 \alpha_k^2 + \frac{1}{2} c_{11} \sum_{k=1}^3 \eta_k^2 + c_{12} \sum_{\substack{j,k=1 \\ j \neq k}}^3 \eta_j \eta_k \right) \quad (2)$$

where σ_k is the mechanical stress. c_{11} and c_{12} are the elastic stiffnesses at constant magnetization. From the condition $\sigma_3 = 0$, which follows from the relaxation of the interlayer distance perpendicular to the film plane. One further obtains:

$$\eta_3 = -\frac{2\eta c_{12} + b_1 \alpha_3^2}{c_{11} + B_1 \alpha_3^2}, \quad (3)$$

From the Poisson's ratio expression $\nu = c_{12}/(c_{11} + c_{12})$, we obtain $c_{12}/c_{11} = \nu/(1 - \nu)$. Where $\nu \approx \frac{1}{3}$ for transition metals[3], which gives $c_{12} = c_{11}/2$. The zero strain anisotropy energy can be further decomposed into bulk and interface contributions, $K_1 = K_1^v + K_1^i/t \approx K_1^i/t$ for thin film limit. By substituting η_3 in Eq. 1, and calculating the energy required to rotate magnetization from in-plane ($\alpha_1 = 1$) to out-of-plane ($\alpha_3 = 1$), we get:

$$E_{MA} = K_{eff} + (1 + \omega) b_1 t \eta + (1 - \omega) \frac{B_1}{2} t \eta^2, \quad (4)$$

where

$$K_{eff} = K_1^i + \omega \frac{b_1^2}{c_{11}} \left(1 + \frac{B_1}{2c_{11}} \right) t, \quad (5)$$

and

$$\omega = c_{11}^2 / (c_{11} + B_1)^2. \quad (6)$$

Orbital resolved band structure

Orbital resolved bands at $\eta = 4\%$, 6% , and 8% are plotted along high symmetry direction in 2-D Brillouin zone as shown in Fig. S1 for Fe-interface and Fig. S2 for Pt-interface. For Fe-interface, majority spins are almost occupied. Most of the perpendicular magneto-crystalline anisotropy (PMA) arises from minority spin channel. For Pt-interface, minority spins are the major contributor to PMA. With increasing compressive strain, Fe and Pt d bands overall shift towards lower energy.

Spin-orbit coupling between d bands

In Table. S1, we provide a list of positive spin-orbit coupling (SOC) between d bands for both Fe- and Pt-interfaces. The strength of the SOC is $\Delta^\alpha = \frac{1}{e_u - e_o}$. Here, e_u and e_o are the energies of unoccupied and occupied bands; $\alpha = +, 0, -$ denotes when $E_{eff} > 0$, $E_{eff} = 0$, and $E_{eff} < 0$, respectively. For Fe-interface, d_{xy} and $d_{x^2-y^2}$ bands couples at \bar{X} providing large PMA at $E_{eff} = 0$. Under $E_{eff} > 0$, this coupling increased up to two times due to band shift towards E_F . Alternatively, due to band shift away from E_F under $E_{eff} < 0$, this coupling reduces. Moreover, d_{xz} and d_{yz} bands also yield large PMA at \bar{M} . For Pt-interface, electric field effects the SOC strength linearly, i.e. $\Delta^- > \Delta^0 > \Delta^+$. d_{xy} and $d_{x^2-y^2}$ bands at \bar{X} shift towards E_F under $E_{eff} < 0$, providing large PMA. However, these bands move away from E_F under $E_{eff} > 0$, reducing PMA contribution.

* Email address: sonny@ulsan.ac.kr

† Email address: schong@ulsan.ac.kr

[1] D. Eastman, Phys. Rev. **148**, 530 (1966).

[2] L. D. Landau and E. M. Lifshitz, *Electrodynamics of Continuous Media (Pergamon Press, Oxford, 1984)* (Pergamon Oxford, 1984).

[3] D. Sander, Rep. Prog. Phys. **62**, 809 (1999).

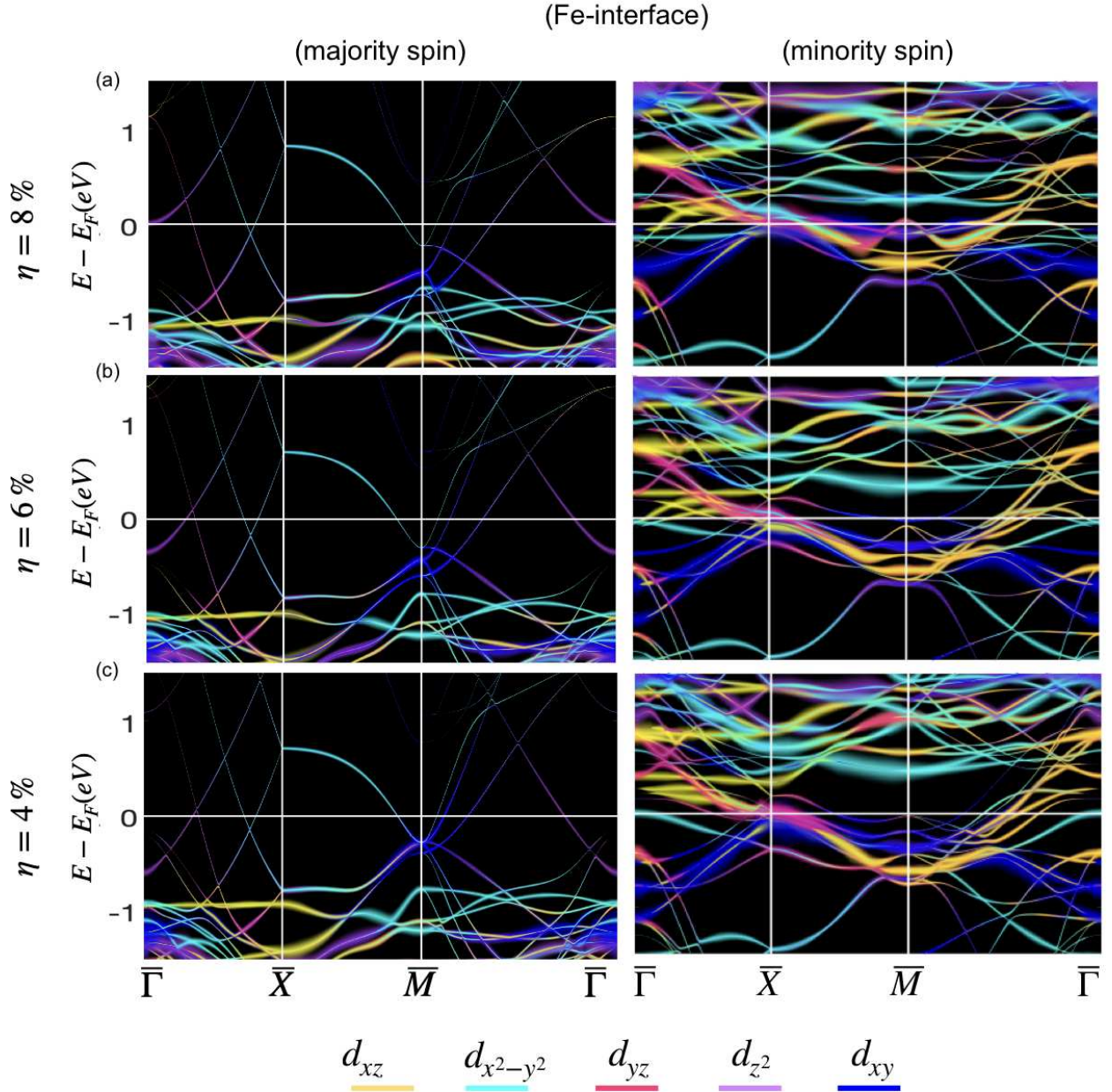


FIG. S1. Orbitally resolved Fe d bands for majority and minority spins along $\bar{\Gamma}$ - \bar{X} - \bar{M} - $\bar{\Gamma}$ direction in 2D Brillouin zone at the FM/I interface for $\eta = 8, 6,$ and 4% , respectively. The reference energy ($E = 0$ eV) places at E_F . Blue, cyan, pink, purple and golden color for $d_{xy}, d_{x^2-y^2}, d_{yz}, d_{z^2}$ and d_{xz} .

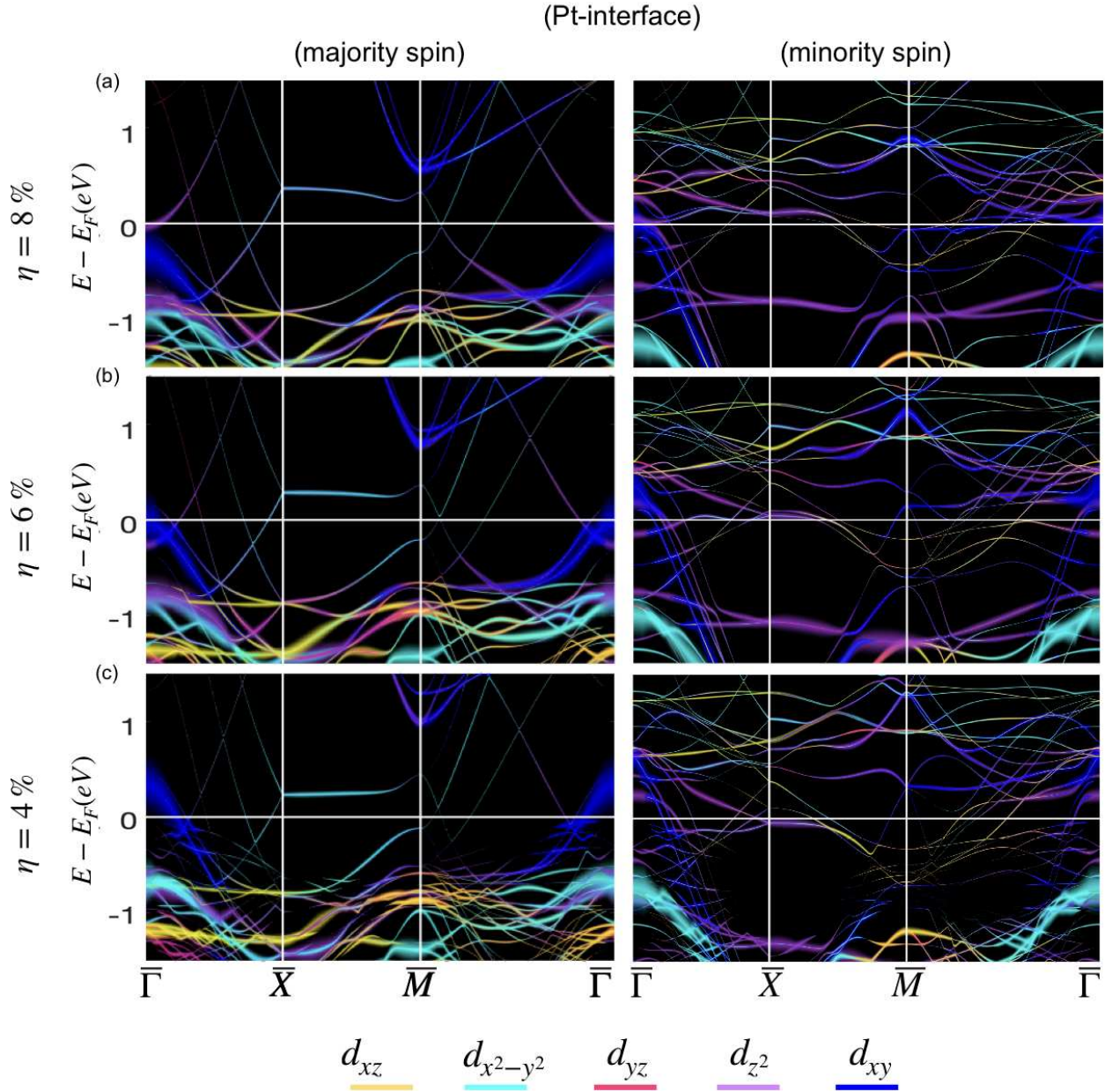


FIG. S2. Orbitally resolved Pt d bands for majority and minority spins, along $\bar{\Gamma}-\bar{X}-\bar{M}-\bar{\Gamma}$ direction in 2D Brillouin zone at the FM/I interface for $\eta = 8, 6$, and 4% , respectively. The reference energy ($E=0$ eV) places at E_F . Blue, cyan, pink, purple and golden color for d_{xy} , $d_{x^2-y^2}$, d_{yz} , d_{z^2} and d_{xz} .

	symmetry point	coupled bands	Δ^-	Δ^0	Δ^+
Fe-interface	\bar{X}	$d_{xy}, d_{x^2-y^2}$	2.558	6.897	12.300
		d_{xz}, d_{yz}	5.540	5.903	6.763
		$d_{xy}, d_{x^2-y^2}$	2.004	2.151	2.015
		d_{xz}, d_{yz}	1.998	2.010	2.109
	\bar{M}	$d_{xy}, d_{x^2-y^2}$	2.782	2.782	2.961
		d_{xz}, d_{yz}	1.024	1.011	1.075
		$d_{xy}, d_{x^2-y^2}$	1.530	1.487	1.541
	$\frac{1}{2}\bar{X}\bar{M}$	$d_{xy}, d_{x^2-y^2}$	1.783	1.700	1.792
		$d_{x^2-y^2}, d_{xy}$	0.000	7.100	0.000
		$d_{xy}, d_{x^2-y^2}$	1.447	1.335	1.475
		d_{xz}, d_{yz}	1.024	1.011	1.065
	Pt-interface	\bar{X}	$d_{xy}, d_{x^2-y^2}$	0.766	0.769
\bar{M}		$d_{x^2-y^2}, d_{xy}$	0.643	0.640	0.638
$\frac{1}{2}\bar{M}\bar{\Gamma}$		$d_{x^2-y^2}, d_{xy}$	0.526	0.524	0.524

TABLE S1. List of SOC strength between different d bands at high symmetry points in 2D BZ for both Fe- and Pt-interface. $\Delta^\alpha = \frac{1}{e_u - e_o}$ represents the strength of SOC, where e_u (e_o) are energies of unoccupied (occupied) band; $\alpha = +, 0, -$ denotes when $E_{eff} > 0$, $E_{eff} = 0$, and $E_{eff} < 0$, respectively.